Rapid Communications

Topological crystalline insulator states in the Ca_2As family

Xiaoting Zhou,[1] Chuang-Han Hsu,[2,3] Tay-Rong Chang,[1,*] Hung-Ju Tien,[1] Qiong Ma,[4] Pablo Jarillo-Herrero,[4] Nuh Gedik,[4] Arun Bansil,[5] Vitor M. Pereira,[2,3] Su-Yang Xu,[4,†] Hsin Lin,[6] and Liang Fu[4,‡]

[1]*Department of Physics, National Cheng Kung University, Tainan 701, Taiwan*
[2]*Department of Physics, National University of Singapore, Singapore 117542*
[3]*Centre for Advanced 2D Materials and Graphene Research Centre, National University of Singapore, Singapore 117546*
[4]*Department of Physics, Massachusetts Institute of Technology, Cambridge, Massachusetts 02139, USA*
[5]*Department of Physics, Northeastern University, Boston, Massachusetts 02115, USA*
[6]*Institute of Physics, Academia Sinica, Taipei 11529, Taiwan*

(Received 14 May 2018; published 4 December 2018)

Topological crystalline insulators (TCIs) are insulating electronic phases of matter with nontrivial topology originating from crystalline symmetries. Recent theoretical advances have proposed new TCI states protected by rotational symmetries and provided powerful guidelines to search for TCIs in real materials. Building upon recent theoretical works, we demonstrate a feasible method to identify new TCI states based on first-principles calculations. We systematically unveil the topological properties of the TCI states in Ca_2As. On both top and side surfaces, we observe topological surface states protected independently by rotational and mirror symmetries. We show that a particular lattice distortion can single out the newly proposed topological protection by the rotational symmetry. As a result, the Dirac points of the topological surface states are moved to generic locations in momentum space away from any high-symmetry lines. Such topological surface states have not been seen before. Moreover, the other family members, including Ca_2Sb, Ca_2Bi, and Sr_2Sb, feature different topological surface states due to their distinct topological invariants. We thus further propose topological phase transitions in the pseudobinary systems such as $(Ca_{1-x}Sr_x)_2As$ and $Ca_2As_xSb_{1-x}$. Our work reveals rich and exotic TCI physics across the Ca_2As family of materials and demonstrates a complete roadmap for uncovering TCIs topological nature based on first-principles calculations. Such a method can be broadly applied in searching for new TCIs.

DOI: 10.1103/PhysRevB.98.241104

Finding new topological phases of matter is a research frontier of modern condensed-matter physics and materials science. Following the discoveries of time-reversal symmetry-protected $\mathcal{Z}_2$ topological insulator states in both two dimensions and three dimensions [1–4], intensive efforts have been devoted to searching for new types of topological band insulators protected by crystal symmetries, or topological crystalline insulators (TCIs) [5]. Although the large number of crystalline space group symmetries suggests the possibility of a wealth of TCI states, surprisingly, for a long time, the theoretically known TCIs were limited to crystals with mirror reflections [5–8] and glide mirror reflections [9–13]. This is in sharp contrast to the rich variety of topological semimetal phases and the many real material platforms [14]. Despite rareness, the SnTe family of materials [15–24] was found to show novel electronic properties such as mirror-protected Dirac surface states [15–17], strain-induced gap opening [18,19], unconventional thermoelectric response [20], in-plane ferroelectricity [22], and robust spin-polarized midgap edge states [23]. Because of the rareness of TCIs and because of the observed novel electronic phenomena in SnTe, it is of great interest to find new TCIs, especially the ones that are protected by symmetries beyond mirror reflections.

Recent work theorized a large new class of TCI states in time-reversal-invariant electron systems with spin-orbit coupling, which are protected by the N-fold ($N = 2,\ 4$, or 6) rotational symmetries [25]. Such rotational symmetry-protected TCIs are predicted to show distinct protected boundary states: The surface normal to the rotational axis hosts N Dirac cones, while any strictly two-dimensional system with the same symmetry necessarily has $2N$ stable Dirac points. In the absence of additional symmetry constraints, these N Dirac cones are related by the N-fold rotational symmetry, and can appear at any generic k points in the surface Brillouin zone. In addition, the side surface parallel to the rotational axis is predicted to host N one-dimensional (1D) helical edge states, connecting the top and bottom surfaces. The existence of such 1D states was theoretically established in other classes of TCIs as well [26–28].

The ubiquitous presence of rotational symmetries in crystals raises the hope that rotational symmetry-protected TCIs are widespread in real materials. However, their topological invariants defined in terms of Wannier center flow [29] are difficult to compute in first-principles calculations. Song *et al.* [30] and Khalaf *et al.* [31], building on earlier works [32–34], found that when certain additional symmetry Y is present, topological invariants of TCIs protected by symmetry X can be inferred by the Y-symmetry eigenvalues of energy

*u32trc00@phys.ncku.edu.tw
†suyangxu@mit.edu
‡liangfu@mit.edu

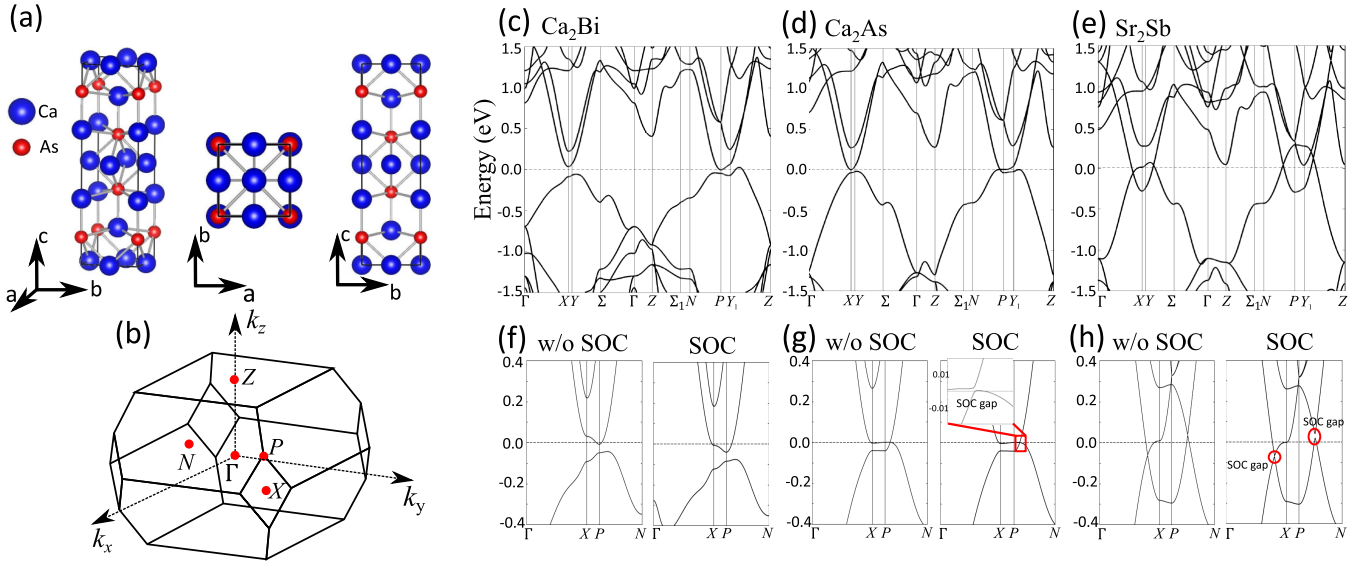

FIG. 1. Lattice and electronic structure of the Ca_2As family. (a) Crystal structure of Ca_2As's body-centered-tetragonal lattice. (b) The corresponding bulk BZ. (c)–(e) Band structures without SOC over a wide energy window. (f)–(h) Zoomed-in band structures both without and with SOC.

bands. Such "symmetry indicator" of nontrivial topology is analogous to the parity criterion for time-reversal invariant in the presence of inversion symmetry [35]. This band symmetry based approach bypasses the numerical difficulty in computing topological invariants directly, thus paving the way for systematic TCI materials search. However, each value of symmetry indicators actually points to several possible topological states.

Building upon these latest theoretical advances [25,27,30–33], we demonstrate a feasible method to identify new TCI states based on first-principles calculations. We systematically unveil the topological properties of the TCI states in Ca_2As. We show that the uncovered novel topological electron states in the Ca_2As family can lead to distinct signatures in various experiments including photoemission, scanning tunneling, transport, optical, and optoelectronic probes, which therefore pave the way for experimental studies on TCI physics.

The first-principles calculations were implemented in the VASP [37] package. The spin-orbit coupling was included self-consistently in the calculations of electronic structures with a Monkhorst-Pack k-point mesh $11\times11\times11$. We use Ca d orbitals and As p orbitals to construct Wannier functions via WANNIER90 [38].

The Ca_2As class of intermetallic materials crystallize in the body-centered-tetragonal lattice system [39]. The space group is $I4/mmm$ (No. 139) and the point group is D_{4h} [39]. The lattice is formed by a $\hat{z}$-direction stacking of alternating two-dimensional (2D) square lattices of Ca or As atoms [Fig. 1(a)]. The available symmetries include $\mathcal{I}$ (space inversion), $4_{(001)}$, $2_{(001)}$, $2_{(100)}$, $2_{(010)}$, $2_{(010)}$, $2_{(110)}$, $2_{(1\bar{1}0)}$, $\mathcal{M}_{(100)}$, $\mathcal{M}_{(010)}$, $\mathcal{M}_{(001)}$, $\mathcal{M}_{(110)}$, and $\mathcal{M}_{(1\bar{1}0)}$ [40]. Figure 1(b) shows the bulk Brillouin zone (BZ). The time-reversal-invariant momenta (TRIM) include one Γ, two X, four N, and one Z, whereas other important non-TRIM high-symmetry points are also noted.

The low-energy electronic structure of all family members is characterized by the two bands close to the Fermi energy [Figs. 1(c)–1(e)]. To examine the band inversion properties of each compound, we first study the band structure in the absence of spin-orbit coupling (SOC). In Ca_2As and Ca_2Sb [Fig. 1(g)], the lowest conduction band (CB) and the highest valence band (VB) are inverted near P (non-TRIM) but remain noninverted at other high-symmetry points. In Sr_2Sb [Fig. 1(h)], the CB and VB are inverted in the vicinity of not only P but also X (TRIM). In Ca_2Bi [Fig. 1(f)], the CB and VB remain noninverted everywhere in the BZ. The above band inversion properties suggest that Ca_2As and Ca_2Sb are pure TCIs, Sr_2Sb is both a weak TI (inverted at two TRIM X points) and a TCI, whereas Ca_2Bi is topologically trivial.

We now study the topology of these compounds by calculating the symmetry-based indicators. According to Ref. [30], band insulators in space group No. 139 are characterized by a pair of indicators $(\mathcal{Z}_2, \mathcal{Z}_8)$. By enumerating of valence electron states in certain irreducible representations at specific high-symmetry points (according to Table I in Ref. [30]), we obtain the following $(\mathcal{Z}_2, \mathcal{Z}_8)$ values: (04) for Ca_2As and Ca_2Sb, (12) for Sr_2Sb, and (00) for Ca_2Bi. In the main text, we will focus on Ca_2As. However, each value of symmetry indicators can point to several different possible topological states. For instance, Table I shows that the symmetry indicator $(\mathcal{Z}_2, \mathcal{Z}_8) = (04)$ indeed points to four possible topological states. Therefore, symmetry indicators alone cannot uniquely determine the topological nature of Ca_2As. Importantly, Table I also shows that the four possible states have different mirror Chern numbers and different rotational symmetry topological invariants. While rotational symmetry topological invariants are difficult to obtain directly, the mirror Chern numbers can be directly calculated by first principles. We therefore calculate the mirror Chern numbers $n_{\mathcal{M}_{(100)}}$, $n_{\mathcal{M}_{(1\bar{1}0)}}$, and $n_{\mathcal{M}_{(001)}}$. Through this way, we uniquely determine each compound's topological state (Table II) from the four possibilities inferred by the $(\mathcal{Z}_2, \mathcal{Z}_8)$ symmetry indicator. We see from Table II that Ca_2As is a pure TCI: It

TABLE I. The four possible topological states for the symmetry indicator $(\mathcal{Z}_2, \mathcal{Z}_8) = (04)$ according to Ref. [30]. $(\nu_0;\nu_1\nu_2\nu_3)$ are the $\mathcal{Z}_2$ invariants for three-dimensional $\mathcal{Z}_2$ TIs. $\nu_0 = 1$ corresponds to a strong TI; $\nu_0 = 0$ but $\nu_1 + \nu_2 + \nu_3 \neq 0$ corresponds to a weak TI. $n_{4_{(001)}}$ is the topological invariant for the fourfold rotational symmetry $4_{(001)}$. This is also a $\mathcal{Z}_2$ invariant. $n_{4_{(001)}} = 1$ corresponds to a rotational symmetry-protected TCI, which features four Dirac surface states on the (001) surface. $n_{\mathcal{M}_{(001)}}$ is the topological invariant for mirror plane $\mathcal{M}_{(001)}$ (the mirror Chern number). This is a $\mathcal{Z}_N$ invariant. $n_{\mathcal{M}_{(001)}} = N$ corresponds to a mirror symmetry-protected TCI, which features N Dirac surface states protected by the $\mathcal{M}_{(001)}$ mirror plane. See Supplemental Material [36] for a detailed introduction to the symmetry indicators and the topological invariants.

$(\nu_0;\nu_1\nu_2\nu_3)$	$n_{4_{(001)}}$	$n_{2_{(100)}}$	$n_{2_{(001)}}$	$n_{2_{(110)}}$	$n_{\mathcal{M}_{(1\bar{1}0)}}$	$n_{\mathcal{M}_{(001)}}$	$n_{\mathcal{M}_{(100)}}$
(0;000)	1	0	0	1	2	0	0
(0;000)	0	0	0	0	0	4	0
(0;000)	1	1	0	0	0	0	2
(0;000)	0	1	0	1	2	4	0

features nontrivial rotational symmetry topological invariants ($n_{4_{(001)}} = 1$ and $n_{2_{(110)}} = 1$) in addition to the nontrivial mirror Chern number $n_{\mathcal{M}_{(1\bar{1}0)}} = 2$. In other words, we demonstrate here that one can uniquely identify a TCI's topological nature (including the rotational symmetry-topological invariants) by combining the calculations of symmetry indicators and the calculations of the mirror Chern numbers.

In order to confirm these bulk topological invariants, we calculate the surface electronic structure of Ca_2As. We first focus on the (001) surface. Since the bulk band inversion occurs near the P point whose surface projection is $\bar{M}$ [Fig. 2(c)], we expect the low-energy electronic structure of the (001) surface band structure to be in the vicinity of $\bar{M}$. Figure 2(a) indeed confirms this case. Zooming in near the $\bar{M}$ point, we observe [Fig. 2(b)] clear surface states (sharp lines) dispersing inside the projected bulk energy gap. Specifically, the surface states form a Dirac point along the $\bar{\Gamma}$-$\bar{M}$ direction in the vicinity of the $\bar{M}$ point. In Fig. 2(d), we show an overview of the topological surface states in the surface BZ: there are four topological Dirac surface states located along the $\bar{M}$-$\bar{\Gamma}$-$\bar{M}$ lines. We check the consistency between the bulk topological invariants and the topological surface states: On the (001) surface, the fourfold rotation ($4_{(001)}$) and the mirror planes ($\mathcal{M}_{(110)}$ and $\mathcal{M}_{(1\bar{1}0)}$) are projected as the $\bar{\Gamma}$ point and the $\bar{M}$-$\bar{\Gamma}$-$\bar{M}$ lines, respectively. By contrast, the twofold rotation $2_{(110)}$ is not respected and thus becomes not important for the (001) surface. Consulting Table II, the nontrivial mirror Chern number ($n_{\mathcal{M}_{(110)}} = n_{\mathcal{M}_{(1\bar{1}0)}} = 2$) requires two Dirac surface states on each mirror line; the nontrivial rotational topological invariant ($n_{4_{(001)}} = 1$) requires four Dirac surface states that are related by the rotational center. Therefore, the obtained surface states are consistent with the bulk topological invariants. On the other hand, the (110) surface shows two surface Dirac cones along the $\tilde{P}$-$\tilde{\Gamma}$-$\tilde{P}$ direction [Figs. 2(e) and 2(f)], which are consistent with the topological invariants $n_{\mathcal{M}_{(1\bar{1}0)}} = 2$ and $n_{2_{(110)}} = 1$. These predicted topological surface states can be detected by photoemission experiments on the Ca_2As family of compounds.

TABLE II. Calculated topological invariants of the Ca_2Sb family.

	$(\nu_0;\nu_1\nu_2\nu_3)$	$n_{4_{(001)}}$	$n_{2_{(100)}}$	$n_{2_{(001)}}$	$n_{2_{(110)}}$	$n_{\mathcal{M}_{(1\bar{1}0)}}$	$n_{\mathcal{M}_{(001)}}$	$n_{\mathcal{M}_{(100)}}$	$\mathcal{I}$
Ca_2As	(0;000)	1	0	0	1	2	0	0	0
Sr_2Sb	(0;111)	1	1	1	1	0	2	0	1
Ca_2Bi	(0;000)	0	0	0	0	0	0	0	0

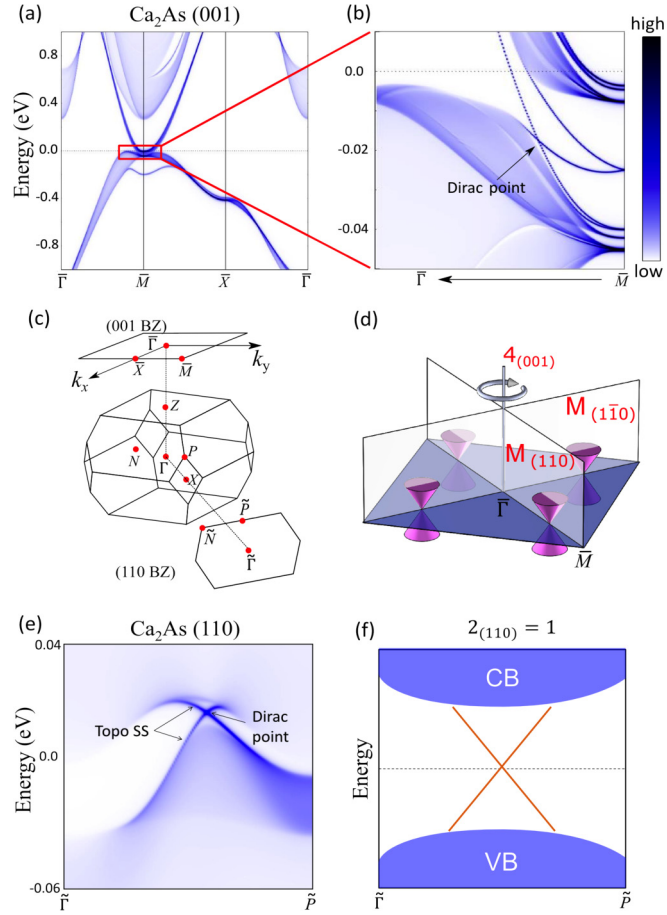

FIG. 2. Topological surface states of Ca_2As on the (001) and (110) surfaces. (a),(b) Calculated surface spectral weight of the (001) surface. The topological surface states along the $\bar{\Gamma}$-$\bar{M}$ line are denoted. (c) The (001) and (110) surface BZs. (d) Schematic illustration for the 4_{001} and $\mathcal{M}_{(110)}$ ($\mathcal{M}_{(1\bar{1}0)}$) topological protection of the surface states. (e) Calculated surface spectral weight of the (110) surface. (f) Schematic illustration for the 2_{110} and $\mathcal{M}_{(1\bar{1}0)}$ topological protection of the surface states.

We now show that a particular kind of lattice distortion can isolate the topological protection by rotational symmetry. The strategy is to identify a particular lattice distortion that can break mirror symmetries while keeping rotational symmetries intact. The rotation-protected topology should remain robust as long as the distortion does not affect the band inversion. As a guideline, we calculated the phonon spectrum and identified phonons in the A_{1g}, E_g, A_{2u}, B_{2u}, and E_u presentations at the Γ point. Our symmetry analysis shows that a distortion according to the B_{2u} modes can break $\mathcal{M}_{(110)}$, $\mathcal{M}_{(1\bar{1}0)}$, and $4_{(001)}$ but preserve $2_{(110)}$ [Fig. 3(a)]. The resulting space group is I-$4m2$ (No. 119). Figure 3 shows the surface band structure

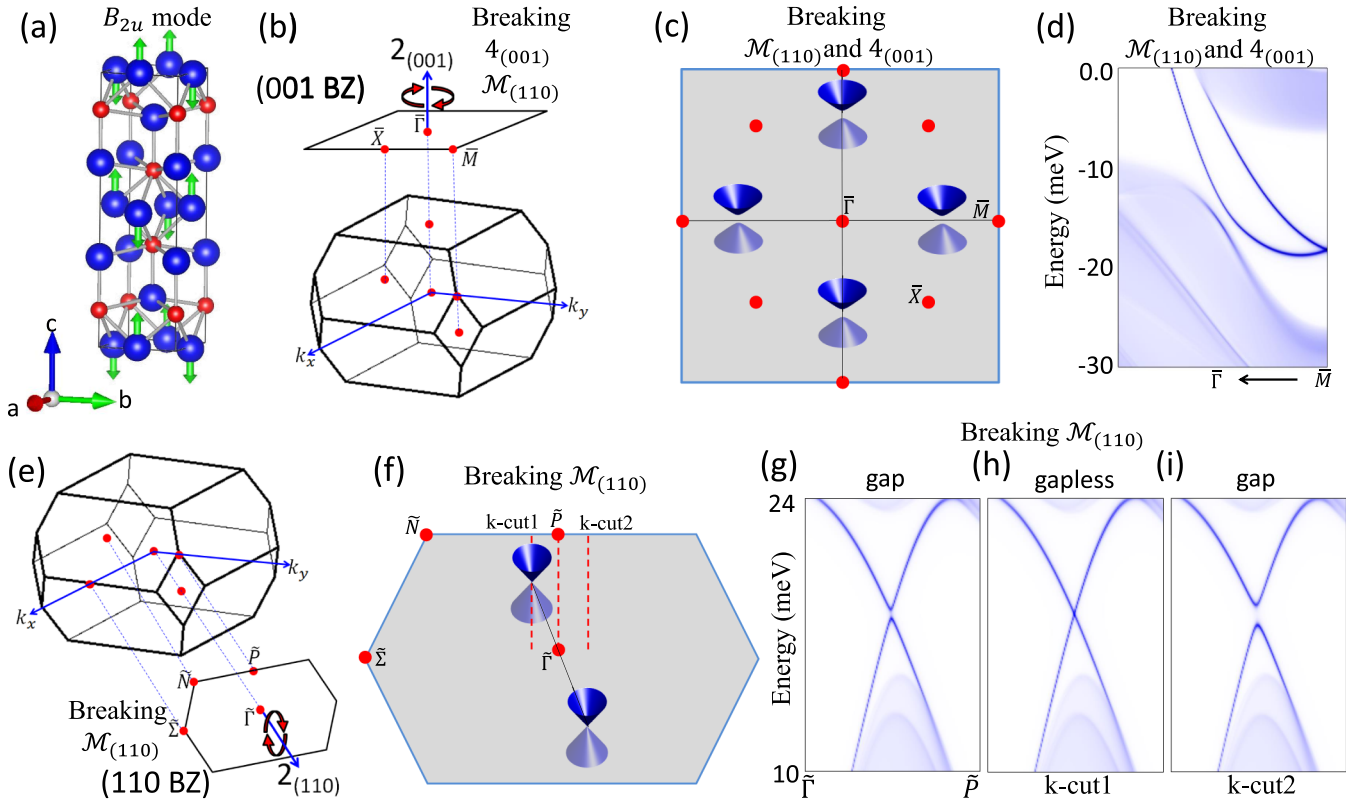

FIG. 3. Isolating the rotational symmetry topological protection by lattice distortion. (a) Atomic displacements according to the B_{2u} distortion. (b) Bulk and (001) top surface BZs after the B_{2u} distortion. (c) Because the $\mathcal{M}_{(110)}$, $\mathcal{M}_{(1\bar{1}0)}$, and $4_{(001)}$ symmetries are broken, all surface Dirac fermions on the (001) surface are expected to gap out. (d) Calculated (001) surface electronic structure after the B_{2u} distortion shows the gap opening of the Dirac fermions. (e) Bulk and (110) BZs after the B_{2u} distortion. (f) Because $\mathcal{M}_{(110)}$, $\mathcal{M}_{(1\bar{1}0)}$ are broken but $2_{(110)}$ is preserved, the surface Dirac fermions on the (110) side surface are expected to remain gapless but move away from the $\tilde{P}$-$\tilde{\Gamma}$-$\tilde{P}$ high-symmetry line to generic k points. (g)–(i) Calculated (110) surface electronic structure after the B_{2u} distortion shows that the Dirac fermions are indeed moved away from generic k points. Note that these dispersion cuts only cover a segment of the surface BZ as noted by the red dotted lines.

after a B_{2u} distortion. Remarkably, we found that all surface Dirac cones on the top (001) surface are gapped [Figs. 3(b)–3(d)]; By contrast, the Dirac cones on the side (110) surface remain gapless but their Dirac points are moved to generic k points off the $\tilde{P}$-$\tilde{\Gamma}$-$\tilde{P}$ line [Figs. 3(e)–3(i)]. These Dirac cones thus represent a new type of topological surface states that are solely protected by the rotational symmetries. The odd-parity phonon can be directly driven by a terahertz optical pulse [41]. Theory also predicted the existence of 1D helical edge states along the side surfaces, which require extremely large computational cost. This can be a direction for future works.

We propose topological phase transitions in the pseudobinary systems. As shown in Fig. 4(a), substituting As for Bi in Ca_2Bi leads to a topological phase transition from a trivial insulator [Ca_2Bi, $(\mathcal{Z}_2\mathcal{Z}_8) = (00)$] to a pure TCI [$Ca_2As$, $(\mathcal{Z}_2\mathcal{Z}_8) = (04)$]. The critical point lies at the doping level $x \simeq 41\%$ [Figs. 4(a)–4(c)]. Through this transition, we expect topological Dirac surface states to emerge at the (001) and (110) surfaces. Similarly, we predict the $Ca_{2-x}Sr_xSb$ system to realize a topological phase transition from a pure TCI [Ca_2Sb, $(\mathcal{Z}_2\mathcal{Z}_8) = (04)$] to a TCI/weak TI [$Sr_2Sb$, $(\mathcal{Z}_2\mathcal{Z}_8) = (12)$]. We found that the critical Sr doping level is roughly at $x \simeq 13\%$ [Figs. 4(e)–4(g)]. We note that the random substitutions in the pseudobinary systems do not preserve the local crystalline symmetries. Therefore, proposed pseudobinary systems also provide a platform to study the robustness of the nontrivial topology against average crystalline symmetries [42].

We thank Chen Fang for valuable discussions on the symmetry indicators. L.F. was supported by the U.S. Department of Energy (DOE), Office of Science, Office of Basic Energy Sciences (BES), Division of Materials Sciences and Engineering (DMSE) under Award No. DE-SC0010526. Q.M. and P.J.-H. were supported by the Center for Excitonics, an Energy Frontier Research Center funded by the DOE, Office of Science, BES under Award No. DESC0001088 and AFOSR Grant No. FA9550-16-1-0382, as well as the Gordon and Betty Moore Foundation's EPiQS Initiative through Grant No. GBMF4541 to P.J.-H., N.G., and S.-Y.X. acknowledge support from DOE, BES DMSE and the Gordon and Betty Moore Foundations EPiQS Initiative through Grant No. GBMF4540. The work at Northeastern University was supported by the US Department of Energy (DOE), Office of Science, Basic Energy Sciences Grant No. DE-FG02-07ER46352, and benefited from Northeastern University's Advanced Scientific Computation Center (ASCC) and the NERSC supercomputing center through DOE Grant No. DE-AC02-05CH11231. H.L.

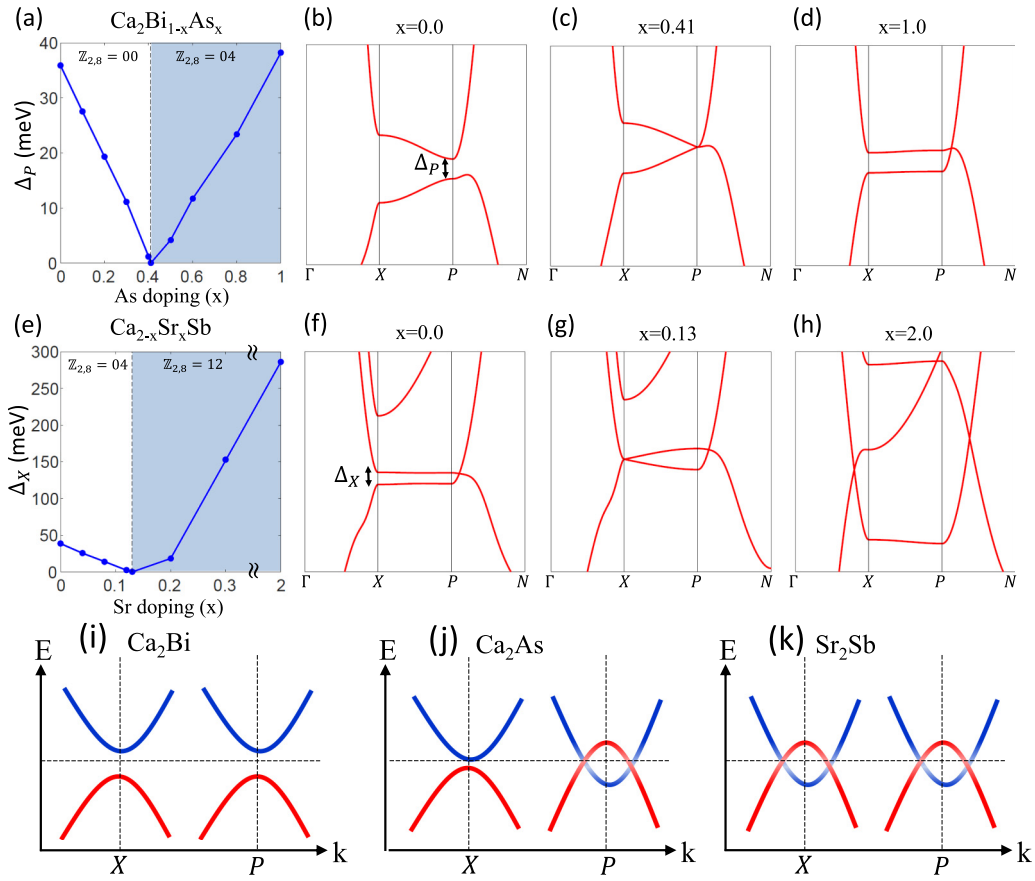

FIG. 4. Topological phase transitions in $Ca_2Bi_{1-x}As_x$ and $Ca_{2-x}Sr_xSb$. (a) Calculated energy gap at the P point in $Ca_2Bi_{1-x}As_x$. (b)–(d) Band structures at different x values. (e) Calculated energy gap at the X point in $Ca_{2-x}Sr_xSb$. (f)–(h) Band structures at different x values. (i)–(k) Schematic electronic states for the representative compounds in the Ca_2As family.

acknowledges Academia Sinica, Taiwan for the support under Innovative Materials and Analysis Technology Exploration (AS-iMATE-107-11). T.-R.C., X.Z., and H.-J.T. were supported from Young Scholar Fellowship Program by Ministry of Science and Technology (MOST) in Taiwan, under MOST Grant for the Columbus Program MOST107-2636-M-006-004, National Cheng Kung University, Taiwan, and National Center for Theoretical Sciences (NCTS), Taiwan.

X. Z., C.-H. H., and T.-R. C. contributed equally to this work.

[1] M. Z. Hasan and C. L. Kane, Rev. Mod. Phys. **82**, 3045 (2010).
[2] X.-L. Qi and S.-C. Zhang, Rev. Mod. Phys. **83**, 1057 (2011).
[3] A. Bansil, H. Lin, and T. Das, Rev. Mod. Phys. **88**, 021004 (2016).
[4] L. Fu, C. L. Kane, and E. J. Mele, Phys. Rev. Lett. **98**, 106803 (2007).
[5] L. Fu, Phys. Rev. Lett. **106**, 106802 (2011).
[6] J. C. Y. Teo, L. Fu, and C. L. Kane, Phys. Rev. B **78**, 045426 (2008).
[7] T. H. Hsieh, H. Lin, J. Liu, W. Duan, A. Bansil, and L. Fu, Nat. Commun. **3**, 982 (2012).
[8] H. Weng, J. Zhao, Z. Wang, Z. Fang, and X. Dai, Phys. Rev. Lett. **112**, 016403 (2014).
[9] B. J. Wieder, B. Bradlyn, Z. Wang, J. Cano, Y. Kim, H.-S. D. Kim, A. Rappe, C. Kane, and B. A. Bernevig, Science **361**, 246 (2018).
[10] Z. Wang, A. Alexandradinata, R. J. Cava, and B. A. Bernevig, Nature (London) **532**, 189 (2016).
[11] K. Shiozaki, M. Sato, and K. Gomi, Phys. Rev. B **91**, 155120 (2015).
[12] K. Shiozaki, M. Sato, and K. Gomi, Phys. Rev. B **93**, 195413 (2016).
[13] K. Shiozaki, M. Sato, and K. Gomi, Phys. Rev. B **95**, 235425 (2017).
[14] B. Yan and C. Felser, Ann. Rev. Condens. Matter Phys. **8**, 337 (2017).
[15] Y. Tanaka, Z. Ren, T. Sato, K. Nakayama, S. Souma, T. Takahashi, K. Segawa, and Y. Ando, Nat. Phys. **8**, 800 (2012).
[16] P. Dziawa, B. Kowalski, K. Dybko, R. Buczko, A. Szczerbakow, M. Szot, E. Łusakowska, T. Balasubramanian, B. M. Wojek, M. Berntsen *et al.*, Nat. Mater. **11**, 1023 (2012).

[17] S.-Y. Xu, C. Liu, N. Alidoust, M. Neupane, D. Qian, I. Belopolski, J. Denlinger, Y. Wang, H. Lin, L. Wray *et al.*, Nat. Commun. **3**, 1192 (2012).
[18] Y. Okada, M. Serbyn, H. Lin, D. Walkup, W. Zhou, C. Dhital, M. Neupane, S. Xu, Y. J. Wang, R. Sankar *et al.*, Science **341**, 1496 (2013).
[19] I. Zeljkovic, Y. Okada, C.-Y. Huang, R. Sankar, D. Walkup, W. Zhou, M. Serbyn, F. Chou, W.-F. Tsai, H. Lin *et al.*, Nat. Phys. **10**, 572 (2014).
[20] T. Liang, Q. Gibson, J. Xiong, M. Hirschberger, S. Koduvayur, R. Cava, and N. Ong, Nat. Commun. **4**, 2696 (2013).
[21] X. Li and Q. Niu, Phys. Rev. B **95**, 241411(R) (2017).
[22] K. Chang, J. Liu, H. Lin, N. Wang, K. Zhao, A. Zhang, F. Jin, Y. Zhong, X. Hu, W. Duan *et al.*, Science **353**, 274 (2016).
[23] P. Sessi, D. Di Sante, A. Szczerbakow, F. Glott, S. Wilfert, H. Schmidt, T. Bathon, P. Dziawa, M. Greiter, T. Neupert *et al.*, Science **354**, 1269 (2016).
[24] T. Liang, S. Kushwaha, J. Kim, Q. Gibson, J. Lin, N. Kioussis, R. J. Cava, and N. P. Ong, Sci. Adv. **3**, e1602510 (2017).
[25] C. Fang and L. Fu, arXiv:1709.01929 (2017).
[26] F. Schindler, A. M. Cook, M. G. Vergniory, Z. Wang, S. S. Parkin, B. A. Bernevig, and T. Neupert, Sci. Adv. **4**, eaat0346 (2018).
[27] Z. Song, Z. Fang, and C. Fang, Phys. Rev. Lett. **119**, 246402 (2017).
[28] A. Matsugatani and H. Watanabe, arXiv:1804.02794.
[29] M. Taherinejad, K. F. Garrity, and D. Vanderbilt, Phys. Rev. B **89**, 115102 (2014).
[30] Z. Song, T. Zhang, Z. Fang, and C. Fang, Nat. Commun. **9**, 3530 (2018).
[31] E. Khalaf, H. C. Po, A. Vishwanath, and H. Watanabe, Phys. Rev. X **8**, 031070 (2018).
[32] B. Bradlyn, L. Elcoro, J. Cano, M. Vergniory, Z. Wang, C. Felser, M. Aroyo, and B. A. Bernevig, Nature (London) **547**, 298 (2017).
[33] H. C. Po, A. Vishwanath, and H. Watanabe, Nat. Commun. **8**, 50 (2017).
[34] J. Kruthoff, J. de Boer, J. van Wezel, C. L. Kane, and R.-J. Slager, Phys. Rev. X **7**, 041069 (2017).
[35] L. Fu and C. L. Kane, Phys. Rev. B **76**, 045302 (2007).
[36] See Supplemental Material at http://link.aps.org/supplemental/10.1103/PhysRevB.98.241104 for an introduction to the symmetry indicators and the topological invariants mentioned in the main text.
[37] G. Kresse and J. Furthmüller, Phys. Rev. B **54**, 11169 (1996).
[38] A. A. Mostofi, J. R. Yates, G. Pizzi, Y.-S. Lee, I. Souza, D. Vanderbilt, and N. Marzari, Comput. Phys. Commun. **185**, 2309 (2014).
[39] A. Hütz and G. Nagorsen, Z. Metallkd. **65**, 618 (1974).
[40] In our notation, $2_{(100)}$ means a twofold rotation about the (100) crystalline axis; $\mathcal{M}_{(100)}$ means a mirror operation that reflects the (100) crystalline direction to $(\bar{1}00)$.
[41] M. Först, R. Mankowsky, and A. Cavalleri, Acc. Chem. Res. **48**, 380 (2015).
[42] L. Fu and C. L. Kane, Phys. Rev. Lett. **109**, 246605 (2012).